19e Journées de l'Hydrodynamique
26 – 28 novembre 2024, Nantes

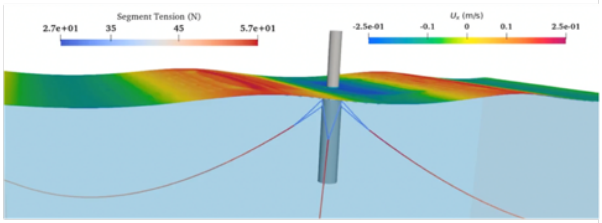

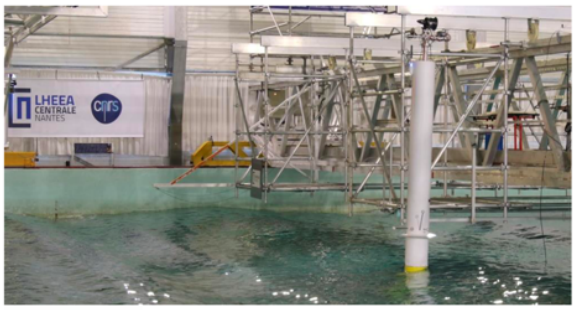

REAL-TIME WAVE FORECASTING IN A PROBABILISTIC FRAMEWORK: FROM FREE SURFACE ELEVATION TO EXCITATION FORCES

PREDICTION DE VAGUES EN TEMPS REEL DANS UN CADRE PROBABILISTE: DE L'ELEVATION DE SURFACE LIBRE AUX EFFORTS SUR LE NAVIRE

E. ANDREEVA[(1)], L. BARTHELEMY[(2)], P. TONA[(1)], A. MERIGAUD[(1)]
ekaterina.andreeva@icloud.com; alexis.merigaud@ifpen.fr

[(1)]IFP Energies Nouvelles, Rueil-Malmaison [(2)]Ecole Nationale Supérieure Maritime, Nantes

Summary

Real-time wave forecasting is a significant technical and scientific challenge. While most of the literature is dedicated to the wave forecasting step *per-se*, i.e. free-surface elevation (FSE) prediction, this study examines how to use those FSE predictions to infer future excitation forces onto a structure at sea. Assuming linear, Gaussian wave theory, we employ a probabilistic approach to derive the mean-square excitation estimation error, given a choice of "input" FSE locations and time interval. Hence, adequate input FSE locations and time durations can be explored, depending on the sea state. Two geometries are studied: a cylinder, and a Wigley hull. Results show that virtually perfect estimates can be obtained from a finite number of input points: from 3 (for the cylinder) to 20-30 (for the ship in relatively short wave lengths), which suggests a connection between the number of necessary points and the complexity of the geometry.

Résumé

La prédiction de vagues en temps réel est un défi scientifique et technique considérable. Alors que la majeure partie de la littérature est consacrée à prédire les vagues elles-mêmes, c'est-à-dire l'élévation de surface libre (ESL), ce travail examine comment utiliser ces prédictions d'ESL pour calculer les futurs efforts hydrodynamiques sur une structure en mer. Sous l'hypothèses de vagues linéaires et Gaussiennes, nous utilisons une approche probabiliste pour calculer l'erreur quadratique moyenne d'estimation des efforts, étant donné un choix d'emplacements et d'intervalle de temps pour les signaux d'ESL d'entrée. Deux géométries sont étudiées : un cylindre et une coque de Wigley. Les résultats montrent qu'une estimation quasi-parfaite peut être obtenue à partir d'un nombre fini de points d'entrée: entre 3 (pour le cylindre) et 20-30 (pour le navire dans des vagues relativement courtes), ce qui suggère un lien entre le nombre de points nécessaires et la complexité de la géométrie.

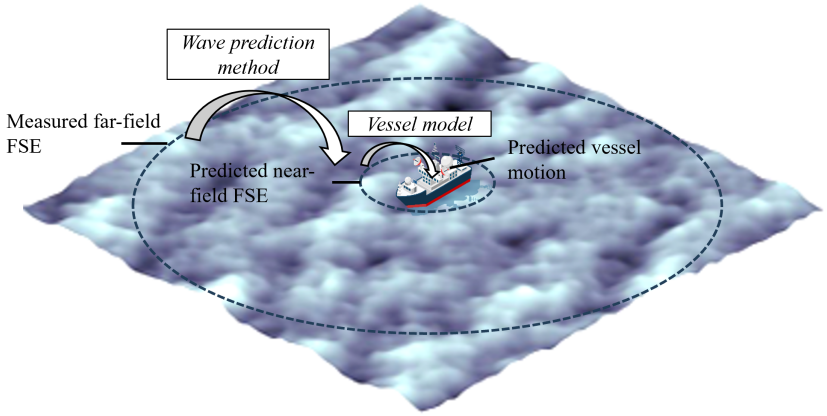

Figure 1: Excitation force prediction in multidirectional waves

I – Introduction

Real-time wave forecasting (RTWF), more often termed deterministic or phase-resolved forecasting, consists in predicting ocean wave-induced motion or forces, from a few seconds to several minutes in advance, using measurements updated in real time. RTWF could show substantial benefits in many coastal and marine applications, by allowing the implementation of predictive control strategies for various tasks such as motion compensation, stabilization and energy harvesting, or by facilitating decision-making in critical offshore operations.

An operational RTWF system typically comprises the following three elements: a sensing system which collects free-surface elevation (FSE) measurements in real time at some distance from the location of interest, a wave prediction method, i.e. a mathematical and numerical procedure which encapsulates the laws of wave propagation to predict the FSE at, or near the location of interest, and finally a vessel dynamical model which relates FSE forecasts to the future vessel or platform motion or forces. The vast majority of the RTWF literature is dedicated to the rather generic wave prediction step; however, for RTWF to be employed in an actual operational scenario, it is essential to extend the forecast to vessel or platform forces and motion, which this work is concerned with.

Assuming that the ship's motion can be described by the Cummins equation, or a non-linear extension thereof [8], calculating wave excitation forces and moments from the predicted FSE is an appropriate first step. In a unidirectional wave field, those can be easily obtained through a convolution of the predicted FSE with the excitation force convolution kernel. In a multidirectional wave field, however (Fig. 1), such a simple approach cannot be applied, since the FSE-to-excitation linear relation is, in general, direction-dependent, and predicting the FSE at a single point does not allow a directional decomposition of the predicted incident waves, as clearly articulated by Kim et al [4].

Some wave prediction approaches, because they are based on a decomposition of the wave field into discrete frequency and directional components, inherently lend themselves to a relatively direct calculation of future excitation forces [4]. But we have been exploring a different route to wave prediction, based on a probabilistic wave model [5, 6], which optimally considers the stochastic nature of ocean waves – among other benefits – but does not provide a decomposition of the wave field into directional components. Therefore, there remains to bridge the gap between the FSE predictions and future wave excitation and induced motion, in our probabilistic prediction framework.

More generally, we consider the problem of inferring excitation forces from a discrete

number of FSE *input points*, near the centre of the structure water plane area (WPA). Such a problem arises for ship motion prediction, as discussed above, but also in wave tank experiments, where it could be desirable to obtain theoretical excitation forces from wave elevation probe measurements, carried out without the structure, as in [4].

Section II outlines how the probabilistic approach of [5] is extended to infer excitation force values from FSE input points. Section III describes the two numerical examples used in this work: a simplified toy-case model, that is, a cylinder of radius 1 m and draft 0.5 m - one of the test-cases of the WAMIT BEM solver[1] - and a representative ship model, with a classical Wigley hull. Results are presented in Sections IV and V for two- and three-dimensional wave fields, respectively. Finally, the main conclusions and avenues for future work are outlined in Section VI.

II – Assumptions and methods

As illustrated in Figure 1, it is assumed that a wave prediction system is implemented, which allows the free-surface elevation (FSE) to be predicted, with arbitrary accuracy, at any desired points in the vicinity of the ship WPA centre. The predicted FSE is assumed to be the *incident* FSE, not the total FSE field – which would also include diffracted and radiated waves. Such an assumption is reasonable e.g. if we consider that the predicted FSE is calculated from measurements in the far-field, where the ship disturbance is negligible. In this study, only the calculation of excitation forces and moments is considered (not the motion), since it would be the common first step in ship motion forecasting, regardless of other modeling assumptions on the ship dynamics.

Assuming linear hydrodynamic theory, the FSE-to-excitation relation is linear, described by a direction- and frequency-dependent transfer function $H_{\eta\to e}(\omega,\theta)$ where ω is the angular frequency and θ is the wave heading. We also note as $h_{\eta\to e}(\tau,\theta)$ the excitation kernel corresponding to $H_{\eta\to e}(\omega,\theta)$. In unidirectional waves with heading θ, as mentioned in the introduction, the excitation force can be trivially calculated from the convolution of $h_{\eta\to e}(\tau,\theta)$ and $\eta(t)$ at the WPA centre, which is possible because, in that case, e is entirely determined from only one, measurable input signal.

However, in a random, directional wave field, such an approach is not possible, because the directional components, that together constitute η, cannot be decomposed exactly. Therefore, throughout this work, the excitation signal is merely *estimated* from FSE signals taken at a finite number of locations, referred to as *input FSE points*. More precisely, the input FSE is taken over a time interval $[\underline{T}_{in};\overline{T}_{in}]$ to infer $e(\tau=0)$, where $\tau=0$ is the present time.

Assuming a Gaussian random wave field [9], with known spectrum, it is possible to calculate the optimal excitation estimate, depending on the chosen input FSE locations, $\underline{T}_{\text{in}}$, $\overline{T}_{\text{in}}$, and the wave spectrum, following the probabilistic approach outlined in [10] and [5]. Although the latter two references are only concerned with predicting the FSE from other FSE measurements, here we extend the approach to accommodate any variables, related to the FSE through a linear transfer function $H(\omega,\theta)$, such as the excitation force.

Indeed, consider any two variables v_i and v_j, related to the FSE through transfer functions $H_i(\omega,\theta)$ and $H_j(\omega,\theta)$, and taken at two locations $\mathbf{x}_i$, $\mathbf{x}_j$ and two instants τ_i, τ_j relative to present time. Then, the covariance $< v_i(\mathbf{x}_i,\tau_i)v_j(\mathbf{x}_j,\tau_j) >$ can be calculated using the Wiener-Khinchine relation [7], applied to the cross-spectrum S_{ij} of variables v_i

[1] https://www.wamit.com/

and v_j:

$$< v_i(\mathbf{x}_i, \tau_i) v_j(\mathbf{x}_j, \tau_j) >= \frac{1}{2\pi} \int_0^{\infty} \int_{\theta=0}^{2\pi} S_{ij}(\omega, \theta) e^{j[\mathbf{k}(\theta,\omega).(\mathbf{x}_j - \mathbf{x}_i) - \omega(\tau_j - \tau_i)]} d\theta d\omega \tag{1}$$

where the cross-spectrum S_{ij} is given by:

$$S_{ij}(\omega, \theta) = S_{\eta\eta}(\omega, \theta) H_i^*(\omega, \theta) H_j(\omega, \theta) \tag{2}$$

Now taking regularly sampled input FSE at a number of input locations $\mathbf{x}_{\text{in},1} ... \mathbf{x}_{\text{in},N}$, a vector of input, "observed" variables is built as:

$$\mathbf{V}_o = [\mathbf{v}_1 \cdots \mathbf{v}_N]^T \tag{3}$$

with

$$\mathbf{v}_n = [\eta(\mathbf{x}_{\text{in},n}, \underline{\mathrm{T}}_{\text{in}}), ... \eta(\mathbf{x}_{\text{in},n}, \overline{T}_{\text{in}})]^T, n = 1...N \tag{4}$$

The vector of output, "predicted" variables reduces to the excitation force at $t = 0$, i.e.:

$$\mathbf{V}_p = [e_{m_1}(\mathbf{0}, 0) \cdots e_{m_M}(\mathbf{0}, 0)]^T \tag{5}$$

where $m_1 \cdots m_M$ are the modes of motion considered, and the WPA centre is assumed to be in $\mathbf{x} = \mathbf{0}$.

Each element of the covariance matrices $\Sigma_{oo} =< \mathbf{V}_o \mathbf{V}_o^T >$, $\Sigma_{op} =< \mathbf{V}_o \mathbf{V}_p^T >$ and $\Sigma_{pp} =< \mathbf{V}_p \mathbf{V}_p^T >$ is filled using Eq. (1), and the optimal estimate of $\mathbf{V}_p$ given available observations $\mathbf{V}_o$ is then given by:

$$\mu_{p|o}(t) = \mathbf{P}\mathbf{V}_o, \text{ with } \mathbf{P} = \Sigma_{po}\Sigma_{oo}^{\dagger} \tag{6}$$

where the † (dagger) superscript denotes the inverse – if Σ_{oo} is full-rank – or a pseudo-inverse – if Σ_{oo} is not full-rank, which indicates that the information in $\mathbf{Z}_o(t)$ is statistically redundant, as shown in [5].

The corresponding prediction error, $\mathbf{E} := \mathbf{P}\mathbf{V}_o - \mathbf{V}_p$, is zero-mean, Gaussian, with covariance $\Sigma_{p|o}$ calculated as follows:

$$\Sigma_{p|o} = \Sigma_{pp} - \Sigma_{po}\Sigma_{oo}^{\dagger}\Sigma_{op} \tag{7}$$

In the rest of this study, the estimated ("predicted") variable is the excitation force (in one ore more modes of motion) at present time $\tau = 0$. The observations are the FSE at a set of input FSE points. The FSE input point locations, the input time interval and the sampling time are all parameters which can be studied. Using the above procedure, the mean square error in excitation estimation can be derived from the chosen input FSE configuration.

III – Numerical examples

Two devices, illustrated in Figure 2, are considered as numerical case studies: a simplified toy case model, that is, a small cylinder of radius 1 m and draft 0.5 m, and a representative ship model, with a classical Wigley hull, see e.g. [3]. The main dimensions of each of the two geometries are summarized in Table 1. Excitation force transfer functions were calculated using WAMIT for the cylinder, and NEMOH for the Wigley hull.

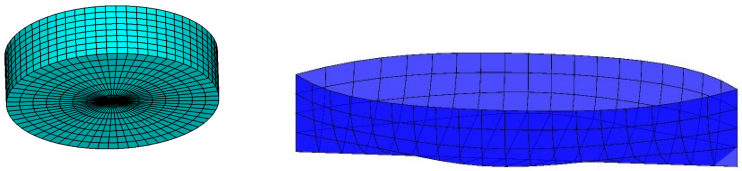

Figure 2: Two structure geometries: a circular cylinder and a Wigley hull.

	Cylinder	Wigley hull
Characteristic dimensions	Radius $R = 1$ m	Width $W = 36.46$ m
	Draft $H = 0.5$ m	Length $L = 116$ m
		Draft $H = 7.2$ m
Convolution time	$T_c = 2.4$ s	$T_c = 35$ s
Sampling time	$\Delta t = 0.06$ s	$\Delta t = 0.5$ s
JONSWAP peak periods	$T_p = \{1, 2, 4\}$ s	$T_p = \{6, 10, 14\}$ s
Peak wave lengths	$\lambda_p = \{1.56, 6.25, 25\}$ m	$\lambda_p = \{56, 156, 306\}$ m

Table 1: Main dimensions of the cylinder and the Wigley hull, together with the range of JONSWAP peak period parameters employed for each device.

For each of the two structures, the estimation of excitation forces is studied in three representative JONSWAP wave spectra [2], with significant wave height $H_{m_0} = 1$m and peak wavelengths both shorter and larger than the structure characteristic length, as documented in Table 1. The spectrum peak enhancement factor is set to $\gamma = 1$. The estimation accuracy is quantified through the normalised mean square error (NMSE), which represents the fraction of excitation signal energy which is not successfully estimated. Therefore, results are independent on the significant wave height.

Considering the convolution kernel $h_{\eta\to e}(\tau)$ for a specific mode of motion, one determines the minimum time T such that $\forall\tau$ with $|\tau| > T$, $h^2_{\eta\to e}(\tau) < \frac{1}{100}\max_{\tau\in\mathcal{R}} h^2_{\eta\to e}(\tau)$. Taking the maximum of those convolution times among all modes of motions provides the value T_c documented in Table 1. Ultimately, $2T_c$ provides an appropriate time scale for the input FSE time interval. Finally, the input FSE is sampled at a time step, also shown in the table, that is small with respect to both the peak wave length and T_c.

IV – Two-dimensional analysis

IV – 1 Uni-directional waves

In a unidirectional wave field, inferring wave excitation from one FSE input location is almost trivial, with or without using the present statistical framework, as discussed in the introduction. If the FSE input location is at the centre of the WPA, then it suffices to perform the convolution of the FSE input with the excitation kernel. If the FSE input location is at some location x, up-wave or down-wave with respect to the WPA centre, then one should consider the kernel of a composite transfer function $H_{\eta_x\to\eta_0}(\omega)H_{\eta\to e}(\omega)$, where $H_{\eta_x\to\eta_0}(\omega) = e^{-ik(\omega)x}$ relates the FSE in x to the FSE in 0.

Alternatively, we can apply the statistical framework of Section II, to explore the effect of FSE input length and location onto excitation reconstruction errors, noting that, if a long enough input FSE length is taken (typically, in the order of $2T_c$), then the statistical

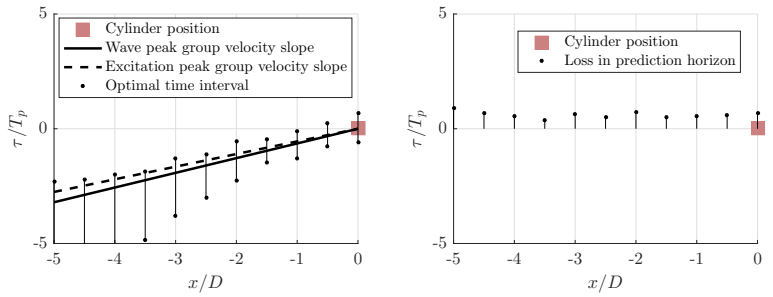

Figure 3: Optimal input FSE time intervals in unidirectional waves for the cylinder, depending on the FSE input location (normalised by the cylinder diameter). $T_p = 2$ s.

approach should yield results identical to the convolution approach. One reason to explore different locations for the input FSE is the non-causality of the excitation kernel [1], which induces a loss in the effective prediction horizon - with respect to the input FSE prediction horizon. By choosing an up-wave input FSE location, the relation between input FSE and excitation can be made causal.

Thus, a number of up-wave FSE input locations are considered, and an optimal input time window is determined, following these three criteria:

- The excitation reconstruction NMSE should be lower than 1%;
- The time window should be as short as possible;
- Among time windows that satisfy the NMSE criterion and have identical length, then the most causal one are chosen.

Results are exemplified for the cylinder in Fig. 3 (left graph) for the pitch degree of freedom, with $T_p = 2$s. They confirm that, by shifting the input FSE location up-wave, the FSE-to-excitation relation is made causal.

However, those benefits are mostly apparent. Indeed, it can reasonably be assumed that the achievable FSE prediction horizon T_H, at the WPA centre, is ultimately governed by the wave sensor range R_{sensor}, following the relation $T_H \approx R_{sensor}/c_{g,p}$, where $c_{g,p}$ is the peak wave group velocity. As a consequence, the FSE at an up-wave location $x < 0$ has a shorter prediction horizon $T_H \approx (R_{sensor} + x)/c_{g,p}$. Thus, while gaining causality by shifting the input FSE up-wave, prediction horizon is lost for the input FSE. After correcting for the latter effect (Fig. 3, right-hand-side graphs), we can see that it is, in fact, difficult to avoid the loss of some prediction horizon. Therefore, in the rest of this work, only FSE input points in the vicinity of the WPA centre will be considered.

IV – 2 Bidirectional waves

Before addressing the three-dimensional wave field, where waves come from multiple directions at the same time, we consider a hypothetical two-dimensional scenario, where waves propagate both backwards and forwards. More precisely, the total wave field is made of two contra-propagating, independent random wave fields, which can be mathematically expressed as follows:

$$\eta(x,t) = \eta_+(x,t) + \eta_-(x,t) \tag{8}$$

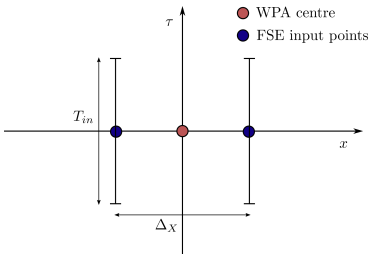

Figure 4: Input FSE configuration in bi-directional waves.

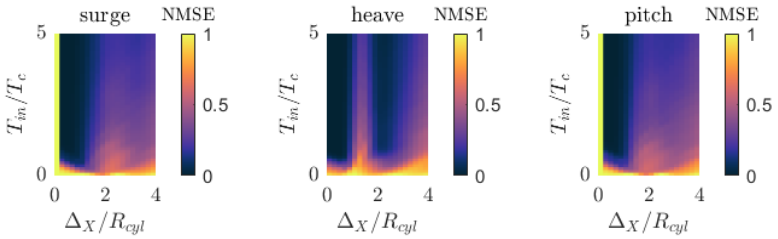

Figure 5: Estimation NMSE for the cylinder, depending on the input point spacing and time interval, with $T_p = 1$s.

where both fields η_+ and η_- are written as Fourier-Stieltjes integrals [9]:

$$\begin{cases} \eta_+(x,t) = \int\limits_{\omega=0}^{\infty} \cos\left(k(\omega)x - \omega t + \phi_+(\omega)\right) \sqrt{S(\omega)d\omega} \\ \eta_-(x,t) = \int\limits_{\omega=0}^{\infty} \cos(-k(\omega)x - \omega t + \phi_-(\omega)) \sqrt{S(\omega)d\omega} \end{cases} \tag{9}$$

and ϕ_+ and ϕ_- are random functions of ω, uniformly distributed in $[0; 2\pi[$, and such that ϕ_+ and ϕ_- at all frequencies are statistically independent from each other.

The excitation forces induced by positively and negatively propagating waves are identical for symmetric modes of motion, in particular heave, but they are reversed for anti-symmetric modes of motion, namely surge and pitch. In mathematical terms, $H_{\eta_+ \to e_i}(\omega) = H_{\eta_- \to e_i}(\omega)$ for $i = 3$, while $H_{\eta_+ \to e_i}(\omega) = -H_{\eta_- \to e_i}(\omega)$ for $i = 1$ or $i = 5$. In that situation, the estimation problem becomes undetermined if only one FSE input point is used, since η cannot be decomposed into its forward and backward components. Therefore, at least two measurement points are necessary, as sketched in Figure 4. Besides, we simplify the analysis by considering a symmetric time window only, and we investigate how the input duration T_{in} and point-to-point distance Δ_X influence the estimation NMSE.

IV – 2.1 Cylinder

Sample NMSE results are shown in Fig. 5 for the cylinder with $T_p = 1$s. From such NMSE maps, it is easy to build the diagrams of Fig. 6, which show possible pairs of symmetrically-arranged pairs of input FSE points, together with the corresponding time interval, which allows for an estimation NMSE lower than 1% in all modes of motion. The results of Fig. 6 show that the two input points should be chosen close to each other, all the more so in shorter wave lengths (Fig. 6a). When the point-to-point spacing increases beyond a short range, the necessary input time eventually increases very rapidly and no reasonable time interval can be found, which satisfies the NMSE criterion.

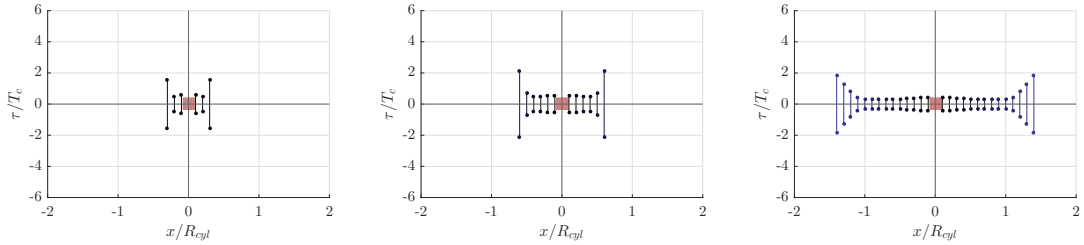

(a) $T_p = 1$s (b) $T_p = 2$s (c) $T_p = 4$s

Figure 6: Bi-directional waves: Input FSE time windows to obtain less than 1% NMSE for the cylinder, with pairs of input FSE locations placed symmetrically with respect to the origin.

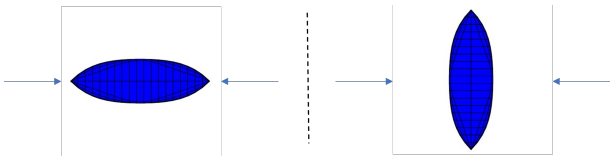

Figure 7: Wigley hull in bi-directional wave fields, for surge, heave and pitch (left) and for sway and roll (right).

IV – 2.2 Wigley hull

For the Wigley hull, surge, heave and pitch, on the one hand, and sway and roll, on the other hand, are treated differently, as illustrated in Figure 7. From the results of Fig. 8, similar conclusions to the cylinder case can be drawn: The two input FSE points should be placed relatively close to each other. Overall, it is interesting to observe that only two input FSE locations are sufficient to resolve the directional ambiguity, and allow for virtually perfect excitation estimates.

V – Three-dimensional wave field

In three dimensions, in a similar manner to the two contra-propagating wave trains of the previous section, an isotropic wave field is considered, where waves propagate without any preferred direction, as illustrated in Fig. 9a. That is expressed mathematically as $S(\omega, \theta) = \frac{1}{2\pi} S_\omega(\omega)$, where $S_\omega(\omega)$ is the direction-integrated spectrum. Considering such an isotropic wave field, although not physically realistic, has several benefits:

- The task of excitation estimation is made as difficult as possible since directional ambiguity is enhanced. Therefore, the accuracy obtained in this hypothetical scenario does not risk to be overly optimistic. In fact, the FSE input configurations obtained in this way should work even better in realistic directional seas, without the need to adapt to a specific directional distribution.

- The analysis is simplified, since modeling assumptions such as the mean wave direction and directional spreading do not need to be taken into account.

Based on the two-dimensional results of Figures 6 and 8, some informed preliminary decisions can be made. First, we set the input time interval to $[-T_c; T_c]$, which should be a conservative choice for all modes of motion. Second, a number of FSE input points are arranged along circles of radius $R_{cyl}/10$ (for the cylinder) and $W/10$ (for the ship), which,

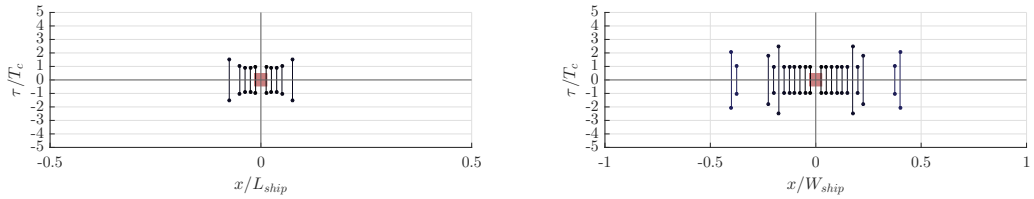

(a) $T_p = 6$ s, surge heave and pitch

(b) $T_p = 6$ s, sway and roll

(c) $T_p = 10$ s, surge heave and pitch

(d) $T_p = 10$ s, sway and roll

(e) $T_p = 14$ s, surge heave and pitch

(f) $T_p = 14$ s, sway and roll

Figure 8: Bi-directional waves: Input FSE time windows to obtain less than 1% NMSE for the Wigley hull, with pairs of input FSE locations placed symmetrically with respect to the origin.

(a) Isotropic distribution.

(b) Mitsuyasu distribution, $s_{max} = 25$.

Figure 9: Wigley hull in three-dimensional JONSWAP sea states with $T_p = 6$ s.

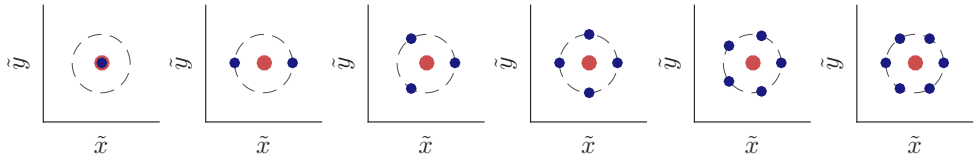

Figure 10: Circular input FSE arrangements for $N_o = 1...6$.

according to Figs. 6 and 8, should be a relevant distance. The first 6 of those circular layouts are illustrated in Fig. 10.

V – 1 Cylinder

For the cylinder, Figs. 11a, 11c and 11e show how the NMSE varies with the number of input FSE points. For heave, only one input point is necessary to obtain accurate estimates, since that mode of motion is insensitive to wave direction due to the hull

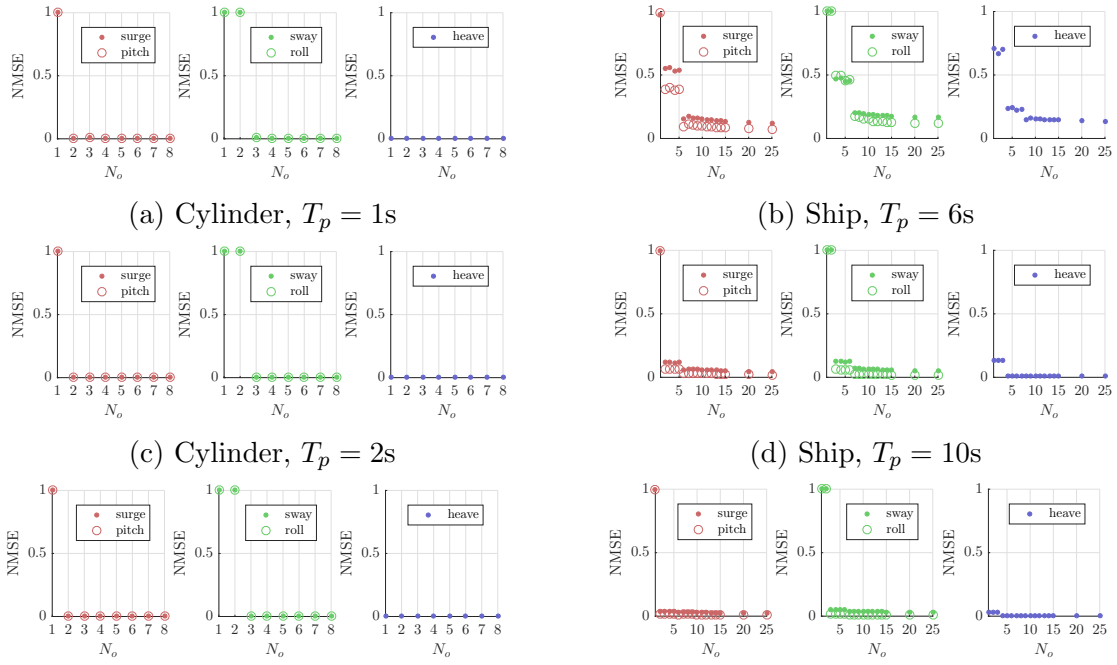

(a) Cylinder, $T_p = 1$s

(b) Ship, $T_p = 6$s

(c) Cylinder, $T_p = 2$s

(d) Ship, $T_p = 10$s

(e) Cylinder, $T_p = 4$s

(f) Ship, $T_p = 14$s

Figure 11: Normalised mean square error accuracy of excitation force estimation, for the cylinder and the Wigley hull, for circular input point arrangements with radius $0.1R_{cyl}$ for the cylinder, and $0.1W_{ship}$ for the ship hull.

axisymmetry. As few as three input points are necessary to obtain accurate estimates in all five modes of motion, regardless of the spectrum considered.

V – 2 Vessel

The striking results, obtained with the cylinder, unfortunately do not seem to extend to the Wigley hull case, as can be appreciated in Figs. 11b, 11d and 11f. In general, the estimation task seems more difficult in shorter waves (Figs. 11b and 11d), where the NMSE does decrease as the number of inputs N_o increases, but the NMSE does not generally approach zero, even for large numbers (20-30) of input locations. Another notable feature of those results is the fact that the NMSE seems to evolve in sudden drops at certain values of N_o, rather than in gradual decrease.

Since the circular arrangement and spacing value, suggested by the two-dimensional analysis, do not seem able to provide accurate excitation estimates in all sea states, several other types of input point arrangements (squares, rectangles, etc.) were considered, mostly through a trial-and-error process, rather than rigorous optimization. Only one of those possibilities is illustrated in the following. The main idea is to use as input the FSE at discrete points within a circle with a chosen radius, while ensuring a homogeneous density of input points. This can be approximately achieved by using "sunflower seed" arrangements[2], illustrated in Figure 12.

Tuning the "sunflower" radius to 0.7 times the hull width, NMSE results are shown in Figure 13. This time, a large enough number of input FSE points allows a virtually perfect excitation force estimate, in all sea states considered and all modes of motion: between approximately 5 ($T_p = 14$ s) and 20 ($T_p = 6$ s). Finally, in the worst-case

[2]See e.g. https://demonstrations.wolfram.com/SunflowerSeedArrangements/ and [11]

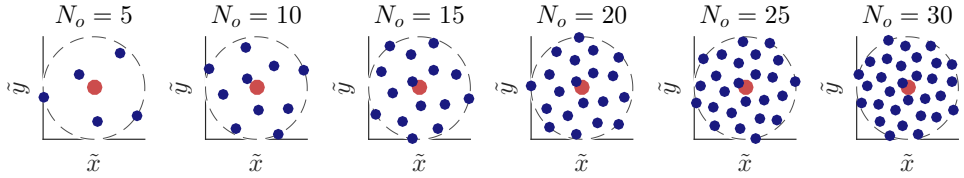

Figure 12: "Sunflower seed" input FSE arrangements for $N_o = 5, 10, ...30$.

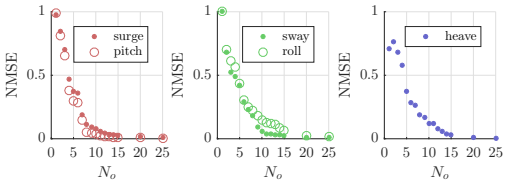

(a) Ship, $T_p = 6$s, isotropic waves.

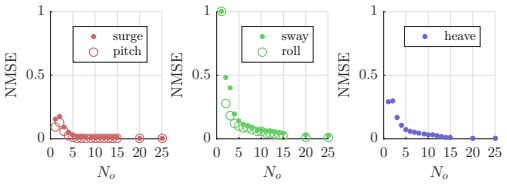

(b) Ship, $T_p = 6$s, directional waves.

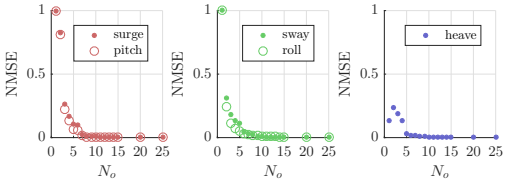

(c) Ship, $T_p = 10$s, isotropic waves.

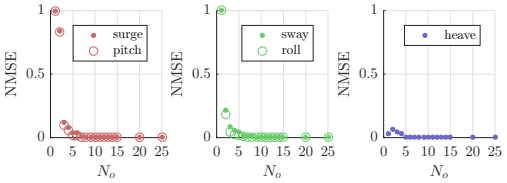

(d) Ship, $T_p = 14$s, isotropic waves.

Figure 13: Normalised mean square error accuracy of excitation force estimation, for the Wigley hull, for "sunflower seed" input point arrangements with radius $0.7W_{ship}$. In fig... Mitsuyasu spreading function with $s_{max} = 25$.

peak period parameter $T_p = 6$ s, Fig. 13b shows the results obtained when the isotropic wave energy distribution is replaced with a Mitsuyasu spreading function with $s_{max} = 25$ (illustrated in Fig. 9b), thus highlighting that realistic directional distributions should be more favorable to the excitation estimation task, compared to our isotropic distribution.

VI – Conclusion

This work does not bring a general and definitive answer to the question initially posed, i.e. that of the number and locations of input FSE measurement locations, necessary to infer the wave excitation forces onto a structure. Yet, a number of trends can be observed.

In a two-dimensional setup with two contra-propagating wave fields, two input points are enough to resolve the wave directional ambiguity, and thus to obtain a virtually perfect excitation force estimation. Those two points should be placed next to each other, i.e. at a distance significantly shorter than the wave peak wave length ($\Delta_X \approx 0.1\lambda_p$). The latter result suggests that using spatial derivatives of the free-surface elevation, as additional inputs to the excitation estimation, could be an interesting avenue for future work.

In a three-dimensional wave field, results seem contrasted, depending on the geometry of the structure considered. In an axisymmetric structure such as the cylinder considered here, as few as three input points, arranged circularly around the WPA centre, suffice to obtain a virtually perfect excitation force calculation – and this encouraging result holds in the hypothetical, worst-case scenario of an isotropic wave field where waves propagate without any preferred direction. The circle radius should be, like in the 2D case, in the order of a tenth of a peak wave length - or smaller.

However, in a more complex geometry, such as the Wigley ship hull considered in

this work, inferring excitation forces in three-dimensional waves can be challenging, and requires a comparatively large number (approximately 20) of input points, for accurate estimates in sea states with short wave lengths. In contrast, longer wave lengths seem to lend themselves better to excitation estimation, necessitating fewer input points. The connection between the geometry complexity and the number of necessary input points, which this work highlights, deserves further investigation.

References

[1] J. Falnes. On non-causal impulse response functions related to propagating water waves. *Applied Ocean Research*, 17(6):379–389, 1995.

[2] K. Hasselmann, T. Barnett, E. Bouws, H. Carlson, D. Cartwright, K. Enke, J. Ewing, H. Gienapp, D. Hasselmann, P. Kruseman, A. Meerburg, P. Muller, D. Olbers, K. Richter, W. Sell, and H. Walden. Measurements of wind-wave growth and swell decay during the Joint North Sea Wave Project (JONSWAP). *Deut. Hydrogr. Z.*, 8:1–95, 01 1973.

[3] I. J. Journé. Experiments and calculations on four Wigley hullforms. *Delft University*, 909, 1992.

[4] I.-C. Kim, G. Ducrozet, V. Leroy, F. Bonnefoy, Y. Perignon, and S. Delacroix. Numerical and experimental investigation on deterministic prediction of ocean surface wave and wave excitation force. *Applied Ocean Research*, 142:103834, 2024.

[5] A. Mérigaud and J. V. Ringwood. Incorporating ocean wave spectrum information in short-term free-surface elevation forecasting. *IEEE Journal of Oceanic Engineering*, 44(2):401–414, 2018.

[6] A. Mérigaud and P. Tona. A stochastic approach to short-term ocean wave forecasting: preliminary results using data from a remote sensing imaging system. In *International Conference on Offshore Mechanics and Arctic Engineering*, volume 85857, page V001T01A012. American Society of Mechanical Engineers, 2022.

[7] A. Papoulis and S. U. Pillai. *Probability, random variables, and stochastic processes*. Tata McGraw-Hill Education, 2002.

[8] T. Perez. *Ship motion control: course keeping and roll stabilisation using rudder and fins*. Springer Science & Business Media, 2006.

[9] W. J. Pierson. A unified mathematical theory for the analysis, propagation and refraction of storm-generated ocean surface waves, part 1 and 2. *NYU, Coll. of Eng., Res. Div.*, 461, 1952.

[10] A. Simanesew, K. Trulsen, H. E. Krogstad, and J. C. N. Borge. Surface wave predictions in weakly nonlinear directional seas. *Applied Ocean Research*, 65:79–89, 2017.

[11] H. Vogel. A better way to construct the sunflower head. *Mathematical biosciences*, 44(3-4):179–189, 1979.